



THE UNIVERSITY *of* EDINBURGH

Edinburgh Research Explorer

Photocatalytic facile ZnO nanostructures for the elimination of the antibiotic sulfamethoxazole in water

Citation for published version:

Makropoulou, T, Kortidis, I, Davididou, K, Motaung, D & Chatzisyseon, E 2020, 'Photocatalytic facile ZnO nanostructures for the elimination of the antibiotic sulfamethoxazole in water', *Journal of Water Process Engineering*, vol. 36, 101299. <https://doi.org/10.1016/j.jwpe.2020.101299>

Digital Object Identifier (DOI):

[10.1016/j.jwpe.2020.101299](https://doi.org/10.1016/j.jwpe.2020.101299)

Link:

[Link to publication record in Edinburgh Research Explorer](#)

Document Version:

Peer reviewed version

Published In:

Journal of Water Process Engineering

General rights

Copyright for the publications made accessible via the Edinburgh Research Explorer is retained by the author(s) and / or other copyright owners and it is a condition of accessing these publications that users recognise and abide by the legal requirements associated with these rights.

Take down policy

The University of Edinburgh has made every reasonable effort to ensure that Edinburgh Research Explorer content complies with UK legislation. If you believe that the public display of this file breaches copyright please contact openaccess@ed.ac.uk providing details, and we will remove access to the work immediately and investigate your claim.



1 **Photocatalytic facile ZnO nanostructures for the elimination of the antibiotic**
2 **sulfamethoxazole in water**

3
4
5 Tatiana Makropoulou^a, Ioannis Kortidis^b, Konstantina Davididou^a, David E. Motaung^{b,c}, Efthalia
6 Chatzisyseon^{a,*}

7
8 ^aSchool of Engineering, Institute for Infrastructure and Environment, University of Edinburgh,
9 The King's Buildings, Edinburgh EH9 3JL, United Kingdom

10 ^bDST/CSIR National Centre for Nanostructured Materials, Council for Scientific and Industrial
11 Research, Pretoria 0001, South Africa

12 ^cDepartment of Physics, University of the Free State, P.O. Box 339, Bloemfontein ZA9300,
13 South Africa

14
15
16
17 *Corresponding Author: e.chatzisyseon@ed.ac.uk; 0044(0)1316505711

20 **Abstract**

21 The degradation of sulfamethoxazole (SMX) by a synthesized ZnO catalyst and under UVA
22 irradiation was examined. ZnO nanostructures were developed by a facile hydrothermal-assisted
23 method. The effect of ZnO heating time and synthesis reaction, pH, catalyst loading, and SMX
24 initial concentration on process efficiency was studied. Water matrices, such as humic acid (HA)
25 solution and surface water (SW), were also used to resemble real environmental water samples.
26 It was observed that when ZnO is synthesized at pH 7.5, nanorods grow on its surface, while
27 nanoplatelets are formed when synthesis takes place at pH 12.5. SMX removal reached 84%
28 after 60 min of treatment in the presence of 200 mg/L ZnO catalyst (8 h-heated at pH 7.5; $C_0 =$
29 10 mg/L). The pseudo-first-order kinetic constants of SMX photodegradation were calculated at
30 0.039, 0.030 and 0.016 min^{-1} for 5, 10, and 20 mg/L SMX, respectively. This decreased
31 efficiency was attributed to the excessive coverage of catalyst surface by SMX molecules,
32 evidenced by SEM micrographs produced after treatment. SMX degradation in SW (12.5%) was
33 considerably lower than in UPW (47.4%) due to the presence of natural organic matter in the
34 first. Interestingly, SMX removal was greatly enhanced in HA matrix (99%) and this can be
35 attributed to the ability of HA to sensitize colloidal ZnO. In all cases, morphological changes of
36 ZnO nanostructures were observed after photocatalytic treatment. It was confirmed that SMX
37 degradation takes place through HO^\bullet by adding HO^\bullet quenchers, such as *tert*-butyl alcohol and
38 methanol, in the reactant mixture.

39

40 **Keywords:** wastewater treatment; pharmaceuticals; priority pollutants; Advanced oxidation;
41 semiconductors; heterogeneous photocatalysis

42 **1. Introduction**

43 Antibiotics are vital for safeguarding human health and have saved millions of lives over the
44 years since their first discovery. Nonetheless, current research indicates that overuse is making
45 antibiotics less effective, since bacteria mutate and develop resistance to them. Antibiotic
46 resistant bacteria (ARB) are developed by mutations emerged from prolonged exposure
47 nullifying antibiotic defense against bacterial infections (Lupo and Coyne, 2012). Therefore, as
48 people continue to overuse antibiotics, as well as over-expose livestock animals to control
49 possible infections, resistant bacteria not only survive but instead thrive. ARB can be found in
50 numerous environments, such as hospitals, waters or crops and are a great challenge in infectious
51 diseases today (Jiang et al., 2013; Giannakis et al., 2018). Each year, ARB infections lead to
52 700,000 deaths globally, while healthcare costs are expected to rise up to 2.9 trillion USD by
53 2050 (OECD, 2016). In addition to the development of ARB, the growing use of antibiotics,
54 exacerbated by their xenobiotic nature, has increased contamination of natural waters and
55 bioaccumulation risk in the food chain (Lupo and Coyne, 2012). For example, sulfamethoxazole
56 (SMX), which is a sulfonamide antibiotic has been widely detected in wastewater treatment plant
57 (WWTP) effluents, surface and drinking water bodies (Fatta-Kassinos et al., 2011; Ribeiro et al.,
58 2016; Lee et al., 2019). SMX is extensively prescribed to treat infectious and respiration diseases
59 in human and veterinary medicine and to promote animal growth (Xekoukoulotakis et al., 2011;
60 Mirzaei et al., 2018b).

61 Currently, when antibiotics enter conventional biological WWTPs, only a small fraction of them
62 is removed (Karaolia et al., 2018). This is due to the fact that existing WWTPs were not
63 originally designed to cope with such persistent contaminants (Fatta-Kassinos et al., 2011;
64 Barbosa et al., 2016). As a result, antibiotics are released into the terrestrial and aquatic

65 environment through disposal or water reuse applications, causing major environmental and
66 health concerns (Martin-Laurent et al., 2019). Finding an effective technology to treat antibiotics
67 in the environment is a major scientific challenge, which has received attention only the last
68 decade.

69 Heterogeneous photocatalysis is an advanced oxidation process (AOP) that can effectively
70 degrade recalcitrant compounds (Byrne et al., 2018; Lee et al., 2019; Lin and Wu, 2019). In
71 principle, irradiation of photocatalysts like ZnO with photons having equal or higher energy level
72 than catalysts' band gap triggers the production of powerful oxidizing species, mainly hydroxyl
73 radicals (HO^\bullet), which can attack organic contaminants (Banerjee et al., 2014), such as antibiotics
74 (Mirzaei et al., 2016), until their final mineralization into CO_2 and inorganic ions. Among
75 various photocatalysts, ZnO has received considerable attention owing to its unique
76 characteristics. ZnO is a semiconductor with a large exciton binding energy of 60 meV and a
77 wide band gap of 3.2 eV at room temperature (Lee et al., 2016). It has the ability to absorb over a
78 larger fraction of the solar spectrum compared to other semiconducting metal oxides, plus it is a
79 biocompatible, non-toxic and low-cost material (Zacharakis et al., 2013; Koutantou et al., 2013;
80 Lee et al., 2016). A way to enhance the photocatalytic activity of a catalyst is by controlling its
81 morphological and structural properties (i.e. surface area, pore size distribution, lattice defects, as
82 well as the predominant crystal facets of the nanostructures). In this study, a low-cost, versatile
83 hydrothermal-assisted technique, applicable at industrial scale, was used to develop ZnO
84 materials with augmented photocatalytic activity.

85 The degradation of SMX by means of photocatalytic oxidation has been widely studied (Abellán
86 et al., 2007; Xekoukoulotakis et al., 2011; Lu et al., 2017; Tomara et al., 2019), however ZnO-
87 mediated photocatalysis has been merely investigated and this only under UVC irradiation. In

88 detail, Pourmoslemi et al. (2016) examined the photocatalytic degradation of SMX over ZnO
89 nanoparticles synthesized by a microwave-assisted gel combustion method. Results showed
90 complete removal of SMX using ZnO nanoparticles/UVC irradiation after 6 hours of treatment.
91 Mirzaei et al. (2018a) achieved 90.4% removal of SMX after 60 min of treatment over a
92 synthesized hierarchical magnetic zinc oxide based composite ZnO@g - C₃N₄ (FZG) when
93 irradiated by UVC light. The same group also studied SMX degradation in the presence of
94 fluorinated ZnO nanoparticles (F-ZnO) and under UVC irradiation obtaining 97% SMX removal
95 after 30 min of treatment (Mirzaei et al., 2018b). Previous studies have demonstrated the
96 efficiency of several ZnO/UVC systems in removing SMX from water, however a study
97 investigating the photocatalytic degradation of SMX by a ZnO/UVA system is still missing from
98 literature. UVA lamps constitute a safer and less energy intensive option than UVC light sources,
99 decreasing the environmental impact of photocatalytic treatment. Furthermore, the wide bandgap
100 of ZnO catalysts is one of their key advantages; ZnO has shown augmented absorbance in the
101 UVA region when compared with the benchmark catalyst P25 TiO₂.

102 To this end, the aim of this work was to investigate the fabrication of ZnO nanostructures and
103 test their photocatalytic activity under UVA irradiation for eliminating SMX antibiotic in water.
104 Parameters affecting the synthesis of ZnO catalysts, such as the heating time and pH of the
105 synthesis reaction, were examined. Key operating factors, including catalyst and SMX initial
106 concentration, as well as the type of the water matrix, were studied in order to assess the
107 efficiency of the process.

108

109 **2. Experimental**

110 **2.1. Materials**

111 Sulfamethoxazole (SMX; $\geq 99\%$ purity, CAS No. 723-46-6) was purchased from Sigma-Aldrich.
112 Leonardite humic acid (HA) IHSS standard was used. HA stock solution was prepared by
113 dissolving a prescribed amount of HA in 0.1 M NaOH and further diluting it in ultra-pure water
114 (UPW; 18.2 M Ω .cm at 25 °C, ELGA LabWater). Surface water (SW) was collected from
115 Blackford Pond (Edinburgh, UK) (TOC = 13.9 mg/L; pH = 6.8 – 7; conductivity = 0.42 mS/cm)
116 and used without pre-treatment. Tert-butyl alcohol and methanol were obtained from Panreac
117 and Sigma-Aldrich, respectively. Commercial ZnO powder Honeywell Fluka was supplied from
118 Fisher Scientific. All reagents used for the synthesis of ZnO catalysts were of analytical grade
119 that were purchased from Sigma-Aldrich and used as received.

120

121 **2.2. ZnO synthesis**

122 ZnO nanostructures were prepared using the facile hydrothermal-assisted process described
123 below. Prior to synthesis, 0.2 M Zn(NO₃)₂·6H₂O was added in 125 mL deionised water and
124 allowed to stir for 2 h at room temperature. While the solution was stirred, approx. 1 M NaOH
125 was added drop-wise to adjust the pH to 7.5, 10.5 or 12.5. After 2 h of stirring, 125 mL of the
126 solution was transferred to an autoclave reactor vessel (stainless steel, volume 200 mL Anton
127 Paar) and synthesized in an oven at 200 °C for specific time intervals ranging from 8 to 48 h.
128 White solid precipitates were attained that were collected by consecutive rinse/centrifugation
129 cycles using deionized water. The final ZnO product was dried at 90 °C for 12 h in air.

130

131 **2.3. Catalyst characterization techniques**

132 The structural features of ZnO were analysed using X-ray powder diffraction (XRD, PANalytical
133 X' pert Pro PW 3040/60, Netherlands) fitted with a Cu radiation ($\lambda = 0.15418$ nm) source. XRD
134 analyses were carried out at 45.0 kV and 40.0 mA, from $2\theta = 20$ to 90° at room temperature. The
135 surface morphology was probed using a field emission scanning electron microscope (SEM,
136 Zeiss-Auriga) at an accelerating voltage of 3 keV. The Brunauer, Emmett and Teller (BET)
137 surface area and N_2 adsorption-desorption isotherms were determined with the use of
138 Micromeritics TRISTAR 3000 (USA). Prior to measurements, ZnO materials were thoroughly
139 degassed at 110°C for 2 h under continuous N_2 gas flow to remove adsorbed contaminants. The
140 optical properties were probed using a photoluminescence spectrometer (Jobin-Yvon Nanolog) at
141 an excitation wavelength of 330 nm using a xenon lamp (see the electronic supplementary
142 information, ESI).

143

144 **2.4. Photocatalytic tests**

145 Experiments were conducted in an immersion well, batch-operated, slurry photoreactor,
146 purchased from Ace Glass (Vineland, NJ, USA). UVA irradiation was provided by an 11 W low-
147 pressure blacklight fluorescent lamp (PLS G23, Casell Lighting), emitting predominantly at $\lambda =$
148 365 nm. Potassium ferrioxalate actinometry was applied for the estimation of the incident photon
149 flux received by the reactant solution, which was found to be $4.98 \cdot 10^{-6}$ Einstein/s. In a typical
150 photocatalytic run, 500 mL of SMX solution were introduced in the photoreactor and the
151 appropriate amount of catalyst was added. The obtained slurry solution was continuously stirred
152 magnetically to ensure uniform dispersion of catalyst powder and dissolved oxygen. At the
153 beginning of each experiment, the solution was stirred in the dark for 30 min considering that a

154 well-adsorbed substrate is more likely to be oxidized by the short-life photogenerated holes on
155 catalyst surface. After that time, the UVA lamp was switched on and samples were withdrawn at
156 regular time intervals, filtered through 0.45 μm polyvinylidene fluoride (PVDF) syringe filters
157 (CM Scientific Ltd) and further analyzed in terms of SMX concentration. All experiments were
158 conducted at room temperature and at the inherent pH of SMX solutions, which remained
159 constant during photocatalytic treatment.

160

161 **2.5. Analytical techniques**

162 SMX concentration in filtrate samples was measured by means of a high performance liquid
163 chromatography (HPLC) system (S200 Pump, S225 Autosampler, Perkin Elmer) coupled with a
164 diode array detector (S200 EP, Perkin Elmer). Separation was performed on a reverse phase C18
165 analytical column (Luna Phenomenex, 5 μm , 250 \times 4.6 mm) in isocratic elution mode. The HPLC
166 method for SMX measurement was obtained from Özkal et al. (2017). The mobile phase was a
167 mixture of acidified water (pH \sim 3) and acetonitrile (60/40, v/v), eluted at a flow rate of 1
168 mL/min. The detection wavelength was set to 270 nm and the injection volume to 40 μL . The
169 retention time of the detected SMX was 6.27 min. Since humic acid (HA) solution with a UV
170 absorbance around 254 nm (Rodríguez et al., 2016) is used in this work as a water matrix, it is
171 important to note that the presence of HA could not interfere with the HPLC method used in this
172 study for SMX detection, and that it had a negligible impact on the separation of SMX.

173

174 3. Results and Discussion

175 3.1. Catalyst characterization

176 Figure 1 displays the XRD patterns of ZnO nanostructures synthesized at different pH at 200 °C
177 for 8 h. All the diffraction peaks can be indexed to the standard wurtzite ZnO form (JCPDS No.
178 36-1451). The absence of additional peaks indicates the lack of impurities, thus validating the
179 quality of the as-prepared ZnO nanostructures. Furthermore, a size-dependent spreading of the
180 curve is observed with the increase of the synthesis pH; a clear peak shift to higher angles takes
181 place, when pH increases from 7.5 to 12.5 (Figure 1b). The average crystallite sizes, estimated
182 by the Scherer formula (Mhlongo et al., 2015), are 39.31 and 33.68 nm for pH 7.5 and 12.5,
183 respectively.

184

185 Figure 1

186

187 The N₂ adsorption/desorption isotherms of ZnO catalysts, shown in Figure 2, reveal a type IV
188 behaviour with pore diameter in the range of 4 – 100 nm. Both S_{BET} and pore diameter depend on
189 the pH of the synthesis reaction; S_{BET} increases from 4.852 ± 0.101 m²/g at pH 7.5 to 7.547 ±
190 0.113 m²/g at pH 12.5 for the same synthesis reaction time of 8 h. This is also confirmed by SEM
191 and XRD analyses (Figures 1 and 3), which reveal reduction of crystallite size and further
192 morphological and textural transformations of ZnO structures at higher reaction pH values.

193

194 Figure 2

195

196 The SEM micrographs of ZnO catalysts are presented in Figure 3. As can be seen in the low
197 resolution of Figure 3a, synthesis of ZnO at pH 7.5, leads to the growth of nanorods on its
198 surface, which are nearly all aligned towards the same direction. The higher resolution inset
199 graph of Figure 3a further reveals the hexagonal nature of these nanorods. The average diameter
200 and length of the nanorods are roughly 50 nm and 1 μm , respectively. ZnO synthesis at higher
201 pH (i.e. 12.5) results in the formation of nanoplatelets with average diameter approx. 75 nm
202 (Figure 3b).

203

204 Figure 3

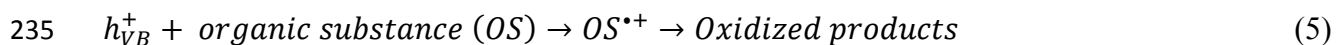
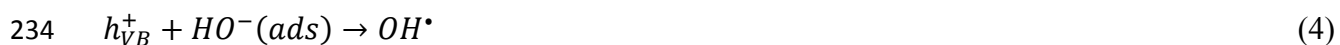
205

206 **3.2. Effect of ZnO synthesis route on SMX degradation**

207 One way to enhance the photocatalytic activity of materials is via morphological and structural
208 modification, which can be achieved by altering synthesis parameters. This study investigates the
209 effect of two key parameters, the pH of the synthesis reaction and the heating time, on the
210 photocatalytic activity of ZnO. Figure 4 shows the degradation of SMX in the presence of ZnO
211 catalysts synthesized at different pH (i.e. 7.5, 10.5 and 12.5) and heated for 24 h at 200 $^{\circ}\text{C}$ during
212 synthesis. As can be seen, the photocatalytic degradation of SMX decreases gradually with the
213 increase of synthesis reaction pH. In detail, SMX removal percentages in the presence of ZnO
214 catalysts synthesized at pH 7.5, 10.5 and 12.5 are 58, 55 and 44%, respectively. The
215 photocatalytic degradation of SMX was found to fit very well with the pseudo-first-order
216 kinetics with the coefficient of linear regression of data fitting, R^2 , being > 0.99 . The pseudo-first-

217 order kinetic constants, k_{app} were calculated at 0.015, 0.013 and 0.009 min^{-1} for SMX
 218 degradation over ZnO synthesized at 7.5, 10.5 and 12.5, respectively. It becomes clear that the
 219 use of ZnO nanostructures synthesized at acidic conditions enhances photocatalytic performance.
 220 This can be explained by the higher relative concentration of lattice defects that is observed at
 221 lower pH values and leads to improved charge transportation and thus higher process efficiency
 222 (Nkosi et al., 2014). Based on the photoluminescence study that was carried out for the ZnO
 223 under study (Figure S1), it is evident that the relative concentration of oxygen vacancies (V_O)
 224 [estimated from the relative intensity of visible emission and ultraviolet ($\text{Vis}(V_O)/\text{UV}$)] decreases
 225 from 6.85 to 4.09 and further to 0.99 as synthesis reaction pH increases from 7.5 to 10.5 and
 226 further to 12.5, respectively.

227 V_O leads to the creation of unpaired electrons acting as donors and it alters the adsorption
 228 behavior of O_2 and H_2O on ZnO surface. The generated pairs of electron holes can directly react
 229 with organic substances, (Eq. (5)), or indirectly by producing free radicals, Eqs. (2)–(4) (Mirzaei
 230 et al., 2016) .



236

237 Figure 4

238

239 The effect of heating time during ZnO synthesis on its photocatalytic activity was then assessed.
240 For this purpose, ZnO catalysts were prepared applying different heating times (i.e. 8, 12, 24,
241 and 48 h) at 200 °C and reaction pH 7.5. As can be seen in Figure 5, the heating time has a
242 negative effect on the ZnO photocatalytic performance. For example, SMX removal in the
243 presence of 8 h-heated ZnO is 84%, after 60 min of treatment, while decreases to 56% when
244 ZnO heated for 48 h is used. Considering that not any structural change occurs during the
245 increase of the synthesis reaction time, this behavior can be attributed to the decrease of the
246 active surface area from $4.852 \pm 0.101 \text{ m}^2/\text{g}$ (at 8 h) to $0.790 \pm 0.104 \text{ m}^2/\text{g}$ (at 48 h) that is
247 observed as the crystallite sizes increase with heating time. As a result, SMX removal decreases,
248 since there is less surface area to facilitate photocatalytic reactions (Wang et al., 2012). This
249 trend can be also justified by the reduction of lattice defects, such as V_{O} , because the crystal
250 quality of the material improves with reaction time.

251 The photocatalytic degradation of SMX was further evaluated in the presence of ZnO (Fluka), at
252 the same operational conditions, to establish a comparison against a commercially available
253 photocatalyst. In this case, 99.9% of SMX was removed within 40 min of treatment. The
254 observed difference in photocatalytic activity can be attributed to the higher adsorption capacity
255 of ZnO (Fluka) compared to the synthesized ZnO materials; after 30 min in the dark, 13.1% of
256 SMX has been adsorbed on ZnO (Fluka), whereas the respective percentages for the novel
257 catalysts are in the range of 1.6 – 7.2%, Adsorption capacity increases with surface area, for that
258 reason ZnO-8h@7.5pH and ZnO-8h@12.5pH, the two catalysts with the highest S_{BET} (Figure 2),
259 are tested in the following experiments to optimize the process and explore their capacity in
260 different water matrices.

261

262 Figure 5

263

264 3.3. Effect of initial concentration of SMX

265 To evaluate the effect of the initial SMX concentration on photocatalytic performance, 5, 10, and
266 20 mg/L of SMX were applied in the presence of 200 mg/L ZnO heated for 8 h at pH 7.5 (noted
267 as ZnO-8h@7.5pH). As can be seen in Figure 6a, when the initial concentration of SMX
268 increases from 5 to 20 mg/L removal efficiency decreases from 90% ($k_{app} = 0.039 \text{ min}^{-1}$) to
269 62.6% ($k_{app} = 0.016 \text{ min}^{-1}$). At a fixed catalyst loading, efficiency is dictated by catalyst's active
270 sites to organic molecules ratio. At relatively low solute concentration, the active sites provided
271 by the semiconductor are in excess and can uptake most of the organic molecules, resulting at
272 higher removal rates. Increase of the initial SMX concentration leads to an excessive coverage of
273 the photocatalyst surface by SMX molecules and reaction by-products, which compete for the
274 active sites of the catalyst, as well as, for the photogenerated hydroxyl radicals, affecting the
275 degradation rates and thus explaining the above findings. SEM graphs of the catalyst after 60
276 min of photocatalytic treatment confirm the extent of surface coverage and further reveal the
277 transformation of surface morphology after contact with organic molecules (in this case SMX)
278 from nanorods (Figure 3a) to nanoparticles (Figure 6b, 6c, 6d). As shown in Figure 6b, after
279 treatment of the solution containing 5 mg/L SMX there are still some nanorods on catalyst
280 surface not yet occupied by SMX molecules However, when the initial concentration of SMX
281 increases to 10 or 20 mg/L, the surface morphology is completely dominated by nanoparticles
282 (Figure 6c and 6d) indicating the complete coverage of catalyst surface by SMX molecules and
283 reaction by-products.

284

285 Figure 6

286

287 **3.4. Effect of catalyst concentration**

288 To investigate the effect of catalyst loading on process efficiency, different concentration of
289 ZnO-8h@7.5pH catalyst (i.e. 100, 150 and 200 mg/L) were used for the degradation of 10 mg/L
290 SMX. SMX removal was found to be 72% ($k_{app} = 0.021 \text{ min}^{-1}$), 73% ($k_{app} = 0.022 \text{ min}^{-1}$) and
291 83% ($k_{app} = 0.03 \text{ min}^{-1}$) in the presence of 100, 150 and 200 mg/L ZnO, respectively after 60 min
292 of treatment (data not shown). At higher amounts of catalyst, the increased number of available
293 active sites results in higher generation of radicals, which are responsible for the photocatalytic
294 oxidation, thus explaining the obtained results (Patil et al., 2010).

295

296 **3.5. Effect of water matrix**

297 Photocatalytic efficiency in environmentally relevant samples, such as surface or waste water,
298 typically varies from that in ultrapure water (UPW) due to the presence of several inorganic and
299 organic constituents that alter degradation kinetics. Humic acid (HA) represents a large fraction
300 of natural organic matter (NOM) in surface waters with concentrations ranging from 2 to 10
301 mg/L (Alrousan et al., 2009). Taking this into account, experiments were carried out in UPW
302 spiked with 2 mg/L HA and in surface water (SW) to assess the effect of water matrix on the
303 photocatalytic removal of SMX. As can be seen in Figure 7, the degradation yield in SW is
304 considerably lower than in UPW; after 60 min of photocatalytic treatment, 47.4% of SMX is
305 degraded in UPW, whereas removal efficiency decreases by almost four times (12.5%) in SW.
306 NOM, HCO_3^- , Cl^- , SO_4^{2-} , PO_4^{3-} , etc., present in SW, may suppress reaction kinetics via

307 competition with SMX for the reactive oxygen species, conversion of hydroxyl radicals into
308 species of lower oxidation potential, and/or adsorption on catalyst surface, thus explaining the
309 obtained results (Rincón and Pulgarin, 2004; Antonopoulou et al., 2015). On the other hand,
310 SMX removal is greatly enhanced in the presence of HA; 10 mg/L of SMX are completely
311 removed within 60 min in HA matrix, which is almost the double yield of that in UPW.
312 Interestingly, the ability of HA to sensitize colloidal ZnO has been previously demonstrated
313 (Selli et al., 1996; Delgado-Balderas et al., 2012). Selli et al. (1996) have shown that HA
314 adsorbed onto the ZnO surface sensitize Cr(VI) photoreduction to Cr(III), as well as, the
315 competitive photoreduction of molecular oxygen leading to hydrogen peroxide, therefore
316 enhancing photocatalytic efficiency. HAs are electron-rich compounds that can easily scavenge
317 the holes produced on semiconductor's valence band, thus reducing the recombination rate of the
318 photogenerated electron-hole pairs. Moreover, electron transfer to the conduction band of the
319 semiconductor may also occur due to the excitation of HAs adsorbed onto catalyst surface upon
320 UV and visible irradiation, accelerating redox reactions and leading to higher reaction rates (Selli
321 et al. 1996). Therefore, the increased SMX degradation rate in the presence of HA might be
322 attributed to the photosensitizing effect of adsorbed HA onto the surface of ZnO nanoparticles.
323 Based on the results shown in Figure 7 (i.e. the huge difference in SMX removal in HA and SW
324 matrices), concerns can arise on whether HA solutions, which are commonly used at lab-scale to
325 simulate natural water matrices (e.g. surface waters), are representative of real environmental
326 conditions. Besides, the long-term exposure to high concentrations (i.e. >50 mg/L) of HA in
327 water has been found to be toxic to endothelial cells and to cause adverse effects on public health
328 (Kihara et al., 2014).

329

330 Figure 7

331

332 To assess the effect of water matrix (i.e. UPW, HA, SW) on catalyst surface, SEM analyses were
333 carried out on the used ZnO materials (Figure 8). It can be observed that after 60 min of
334 photocatalytic treatment in the presence of several organic substances (i.e. SMX, HA or NOM),
335 all nanoplatelets of the pristine ZnO materials (Figure 3b) have transformed into nanoparticles.
336 Nevertheless, differences are observed in the size and the texture of the nanoparticles. For
337 example, when 10 mg/L SMX is treated in HA matrix (Figure 8c) the size of the nanoparticles is
338 bigger than in the case of SMX treatment in UPW (Figure 8a), and this is also confirmed by the
339 evolution of crystallite size after photocatalysis, as shown in Figure 9. Moreover, when SMX is
340 treated in SW matrix (Figure 8e), nanoplatelets are altered to fluffy nanoparticles showing some
341 porous behaviour. Also, while the morphology of ZnO in Figure 8e has changed to nanoparticles,
342 its texture is different than that of SW alone (Figure 8d), since nanoparticles form an island on
343 catalyst surface.

344

345 Figure 8

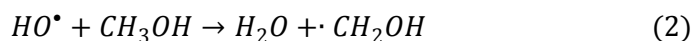
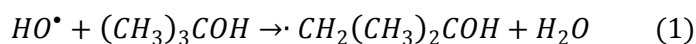
346

347 Figure 9

348

349 **3.6. Oxidation mechanism**

350 Additional experiments were carried out in the presence of HO[•] quenchers to evaluate the
351 contribution of HO[•] on the photocatalytic degradation of SMX. For this purpose, solution of 1 M
352 *tert*-butyl alcohol or methanol was used. HO[•] react with *tert*-butyl alcohol and methanol
353 according to Eqs. (6) and (7), respectively. SMX degradation was found to be negligible in the
354 presence of *tert*-butyl alcohol or methanol (data not shown) suggesting that HO[•] are the major
355 oxidizing species. Furthermore, it was observed that SMX removal, after 60 min of treatment,
356 was slightly higher in the presence of *tert*-butyl alcohol (i.e. 20%) than methanol (i.e. 7%). This
357 is probably due to the fact that methanol reacts at a higher rate with HO[•] ($k' = 9.7 \cdot 10^8 \text{ M}^{-1} \text{ s}^{-1}$, Eq.
358 (7)) than *tert*-butyl alcohol ($k' = (3.8-7.6) \cdot 10^8 \text{ M}^{-1} \text{ s}^{-1}$, Eq. (6)) (Matta et al., 2011), quenching
359 HO[•] faster and thus leaving very few available to react with other organics (i.e. SMX) even from
360 the beginning of treatment.



361

362 4. Conclusions

363 This work reports for first time the degradation of sulfamethoxazole (SMX) under UVA
364 irradiation and over novel ZnO nanomaterials. It was found that the pH of the ZnO synthesis
365 solution significantly affects the morphology of the prepared catalysts and consequently their
366 photocatalytic activity. SMX photo-degradation fits well with pseudo-first-order reaction
367 kinetics, while photocatalytic efficiency increases when the initial SMX concentration is
368 decreased. In all cases, it was observed that after photocatalytic treatment of organic molecules
369 (i.e. SMX, humic acids or natural organic matter), the nanostructure of the catalyst surface was
370 altered from nanorods (or nanoplatelets) to nanoparticles. SMX degradation was assessed in

371 humic acid solution (HA) and surface water (SW) to resemble real environmental conditions. It
372 was found that SMX removal was substantially decreased in SW but greatly enhanced in HA due
373 to the photosensitizing effect of adsorbed HA onto the surface of ZnO nanoparticles, thus raising
374 concerns on whether HA can be widely adopted as a simulant of natural waters (e.g. SW).
375 Considering the encouraging results obtained with the use of the ZnO materials under study,
376 future work should consider the identification of the reaction by-products formed during the
377 photocatalytic degradation of SMX under UVA irradiation and the corresponding toxicity
378 evolution.

379

380

381 **References**

382 Abellán M.N., Bayarri B., Giménez J., Costa J., Photocatalytic degradation of sulfamethoxazole
383 in aqueous suspension of TiO₂, *Appl. Catal. B Environ.* 74 (2007) 233–241.

384 Alrousan D., Dunlop P.S.M., McMurray T.A., Byrne J.A., Photocatalytic inactivation of *E. coli*
385 in surface water using immobilised nanoparticle TiO₂ films, *Water Res.* 43 (2009) 47–54.

386 Antonopoulou M., Skoutelis C.G., Daikopoulos C., Deligiannakis Y., Konstantinou I.K., Probing
387 the photolytic-photocatalytic degradation mechanism of DEET in the presence of natural
388 or synthetic humic macromolecules using molecular-scavenging techniques and EPR
389 spectroscopy, *J. Environ. Chem. Eng.* 3 (2015) 3005–3014.

390 Banerjee S., Pillai S.C., Falaras P., O'shea K.E., Byrne J.A., Dionysiou D.D., New insights into
391 the mechanism of visible light photocatalysis, *J. Phys. Chem. Lett.* 5 (2014)

392 Barbosa M.O., Moreira N.F.F., Ribeiro A.R., Pereira M.F.R., Silva A.M.T., Occurrence and
393 removal of organic micropollutants: An overview of the watch list of EU Decision
394 2015/495, *Water Res.* 94 (2016) 257–279.

395 Byrne C., Subramanian G., Pillai S.C., Recent advances in photocatalysis for environmental
396 applications, *J. Environ. Chem. Eng.* 6 (2018) 3531–3555.

397 Delgado-Balderas R., Hinojosa-Reyes L., Guzmán-Mar J.L., Garza-González M.T., López-
398 Chuken U.J., Hernández-Ramírez A., Photocatalytic reduction of Cr(VI) from agricultural
399 soil column leachates using zinc oxide under UV light irradiation, *Environ. Technol.* 33
400 (2012) 2673–2680.

401 Fatta-Kassinos D., Meric S., Nikolaou A., Pharmaceutical residues in environmental waters and
402 wastewater: Current state of knowledge and future research, *Anal. Bioanal. Chem.* 399
403 (2011) 251–275.

404 Giannakis S., Le T.T.M., Entenza J.M., Pulgarin C., Solar photo-Fenton disinfection of 11
405 antibiotic-resistant bacteria (ARB) and elimination of representative AR genes. Evidence
406 that antibiotic resistance does not imply resistance to oxidative treatment, *Water Res.* 143
407 (2018) 334–345.

408 Jiang H., Zhang D., Xiao S., Geng C., Zhang X., Occurrence and sources of antibiotics and their
409 metabolites in river water, WWTPs, and swine wastewater in Jiulongjiang River basin,
410 south China, *Environ Sci Pollut Res* 20 (2013) 9075–9083.

411 Karaolia P., Michael-Kordatou I., Hapeshi E., Drosou C., Bertakis Y., Christofilos D., Armatas
412 G.S., Sygellou L., Schwartz T., Xekoukoulotakis N.P., Fatta-Kassinos D., Removal of
413 antibiotics, antibiotic-resistant bacteria and their associated genes by graphene-based

414 TiO₂ composite photocatalysts under solar radiation in urban wastewaters, *Appl. Catal. B*
415 *Environ.* 224 (2018) 810–824. doi:10.1016/j.apcatb.2017.11.020.

416 Kihara Y, Yustiawati, Tanaka M, Gumiri S, Ardianor, Hosokawa T, Tanaka S, Saito T, Kurasaki
417 M, Mechanism of the Toxicity Induced by Natural Humic Acid on Human Vascular
418 Endothelial Cells, *Environ Toxicol* 29(8) (2014) 916 – 925.

419 Koutantou V., Kostadima M., Chatzisyneon E., Frontistis Z., Binas V., Venieri D., Mantzavinos
420 D., Solar photocatalytic decomposition of estrogens over immobilized zinc oxide, *Catal.*
421 *Today.* 209 (2013) 66–73.

422 Lee K.M., Lai C.W., Ngai K.S., Juan J.C., Recent developments of zinc oxide based
423 photocatalyst in water treatment technology: A review, *Water Res.* 88 (2016) 428–448.

424 Lee S.-H., Kim K.-H., Lee M., Lee B.-D., Detection status and removal characteristics of
425 pharmaceuticals in wastewater treatment effluent, *J Water Process Eng.* 31 (2019).

426 Lin C.-C., Wu M.-S., Performance of a large reactor in degrading sulfamethazine in water using
427 UV and persulfate, *J Water Process Eng.* 31 (2019).

428 Lu N., Yeh Y.-P., Wang G.-B., Feng T.-Y., Shih Y., Chen D., Dye-sensitized TiO₂-catalyzed
429 photodegradation of sulfamethoxazole under blue or yellow light, *Environ Sci Pollut Res*
430 24 (2017) 489–499.

431 Lupo A., Coyne S., Berendonk T.U., Origin and evolution of antibiotic resistance: the common
432 mechanisms of emergence and spread in water bodies, *Front. Microbiol.* 3 (2012) 18.

433 Martin-Laurent F., Topp E., Billet L., Batisson I., Malandain C., Besse-Hoggan P., Morin S.,
434 Artigas J., Bonnineau C., Kergoat L., Devers-Lamrani M., Pesce S., Environmental risk

435 assessment of antibiotics in agroecosystems: ecotoxicological effects on aquatic microbial
436 communities and dissemination of antimicrobial resistances and antibiotic biodegradation
437 potential along the soil-water continuum, *Environ. Sci. Pollut. Res.* 26 (2019) 18930–
438 18937.

439 Matta R., Tlili S., Chiron S., Barbati S., Removal of carbamazepine from urban wastewater by
440 sulfate radical oxidation, *Environ. Chem. Lett.* 9 (2011) 347–353.

441 Mhlongo G.H., Motaung D.E., Kortidis I., Mathe N.R., Ntwaeaborwa O.M., Swart H.C.,
442 Mwakikunga B.W., Ray S.S., Kiriakidis G., A study on the sensing of NO₂ and O₂
443 utilizing ZnO films grown by aerosol spray pyrolysis, *Mater. Chem. Phys.* 162 (2015)
444 628–639.

445 Michael I., Rizzo L., McArdell CS., Manaia CM., Merlin C., Schwartz T., Dagot C., Fatta-
446 Kassinos D., Urban wastewater treatment plants as hotspots for the release of antibiotics
447 in the environment: a review, *Water Res.* 47 (2013) 957–995.

448 Mirzaei A., Chen Z., Haghghat F., Yerushalmi L., Removal of pharmaceuticals and endocrine
449 disrupting compounds from water by zinc oxide-based photocatalytic degradation: A
450 review, *Sustain. Cities Soc.* 27 (2016) 407–418.

451 Mirzaei A., Yerushalmi L., Chen Z., Haghghat F., Photocatalytic degradation of
452 sulfamethoxazole by hierarchical magnetic ZnO@g-C₃N₄: RSM optimization, kinetic
453 study, reaction pathway and toxicity evaluation, *J. Hazard. Mater.* 359 (2018a) 516–526.

454 Mirzaei A., Yerushalmi L., Chen Z., Haghghat F., Guo J., Enhanced photocatalytic degradation
455 of sulfamethoxazole by zinc oxide photocatalyst in the presence of fluoride ions:
456 Optimization of parameters and toxicological evaluation, *Water Res.* 132 (2018b) 241–

457 251.

458 Nkosi SS., Kortidis I., Motaung DE., Makgwane PR., Ndwandwe OM., Ray SS., Kiriakidis G.,
459 An instant photo-excited electrons relaxation on the photo-degradation properties of
460 TiO₂-x films., *J. Photochem. Photobiol. A Chem.* 293 (2014) 72–80.

461 OECD, Antimicrobial Resistance: Policy Insights, OECD. (2016).

462 Özkal C.B., Frontistis Z., Antonopoulou M., Konstantinou I., Mantzavinos D., Meriç S.,
463 Removal of antibiotics in a parallel-plate thin-film-photocatalytic reactor: Process
464 modeling and evolution of transformation by-products and toxicity, *J. Environ. Sci.* 60
465 (2017) 114–122.

466 Patil A.B., Patil K.R., Pardeshi S.K., Ecofriendly synthesis and solar photocatalytic activity of S-
467 doped ZnO, *J. Hazard. Mater.* 183 (2010) 315–323.

468 Pourmoslemi S., Mohammadi A., Kobarfard F., Assi N., Photocatalytic removal of two antibiotic
469 compounds from aqueous solutions using ZnO nanoparticles, *Desalin. Water Treat.* 57
470 (2016) 14774–14784.

471 Ribeiro R.S., Frontistis Z., Mantzavinos D., Venieri D., Antonopoulou M., Konstantinou I., Silva
472 A.M.T., Faria J.L., Gomes H.T., Magnetic carbon xerogels for the catalytic wet peroxide
473 oxidation of sulfamethoxazole in environmentally relevant water matrices, *Appl. Catal. B*
474 *Environ.* 199 (2016) 170–186.

475 Rincón A.G., Pulgarin C., Effect of pH, inorganic ions, organic matter and H₂O₂ on E. coli K12
476 photocatalytic inactivation by TiO₂: Implications in solar water disinfection, *Appl. Catal.*
477 *B Environ.* 51 (2004) 283–302.

478 Rodríguez F.J., Schlenger P., García-Valverde M., Monitoring changes in the structure and
479 properties of humic substances following ozonation using UV-Vis, FTIR and ¹H NMR
480 techniques, *Science of The Total Environment* 541 (2016) 623-637.

481 Selli E., De Giorgi A., Bidoglio G., Humic acid-sensitized photoreduction of Cr(VI) on ZnO
482 particles, *Environ. Sci. Technol.* 30 (1996) 598–604.

483 Tomara T., Frontistis Z., Petala A., Mantzavinos D., Photocatalytic performance of Ag₂O
484 towards sulfamethoxazole degradation in environmental samples, *J Environ Chem Engin*
485 7 (2019) 103177.

486 Wang Z.X. W., Lu C., Ni Y., Su M., Huang W., Preparation and characterization of visible-light-
487 driven N–F–Ta tri-doped TiO₂ photocatalysts., *Appl. Surf. Sci.* 258 (2012) 8696–8703.

488 Xekoukoulotakis N.P., Drosou C., Brebou C., Chatzisyneon E., Hapeshi E., Fatta-Kassinou D.,
489 Mantzavinos D., Kinetics of UV-A/TiO₂ photocatalytic degradation and mineralization of
490 the antibiotic sulfamethoxazole in aqueous matrices, *Catal. Today.* 161 (2011) 163–168.

491 Zacharakis A., Chatzisyneon E., Binas V., Frontistis Z., Venieri D., Matzavinos D., Solar
492 photocatalytic degradation of bisphenol A on immobilized ZnO or TiO₂, *Int. J.*
493 *Photoenergy.* (2013).

494

495 **List of Figures**

496 **Figure 1.** (a) XRD patterns of ZnO nanostructures synthesized at pH 7.5 and 12.5, and (b) high
497 magnification showing a (101) plane with peak shift.

498 **Figure 2.** The N₂ adsorption/desorption isotherms of ZnO prepared at pH (a) 7.5 and (b) 12.5.

499 **Figure 3.** SEM micrographs of ZnO nanostructures prepared at (a) pH 7.5 and heated for 8 h,
500 and (b) pH 12.5 and heated for 8 h.

501 **Figure 4.** Effect of the pH of the ZnO synthesis reaction on the photocatalytic degradation of
502 SMX ($C_0 = 10$ mg/L, $C_{ZnO} = 200$ mg/L, ZnO heating time: 24 h).

503 **Figure 5.** Effect of catalyst's heating time at 200 °C on the photocatalytic degradation of SMX
504 ($C_0 = 10$ mg/L, $C_{ZnO} = 200$ mg/L, catalysts' synthesis reaction pH = 7.5).

505 **Figure 6.** (a) Effect of initial SMX concentration on its photocatalytic degradation (ZnO-
506 8h@7.5pH, $C_{ZnO} = 200$ mg/L), (b) SEM micrographs of ZnO-8h@7.5pH after 60 min of
507 treatment at initial SMX concentration of 5 mg/L, (c) 10 mg/L, and (d) 20 mg/L.

508 **Figure 7.** Effect of water matrix on the photocatalytic degradation of SMX ($C_0 = 10$ mg/L, C_{ZnO}
509 = 200 mg/L, catalyst: ZnO-8h@12.5pH).

510 **Figure 8.** SEM micrographs of ZnO-8h@12.5pH after 60 min of treatment in the presence of (a)
511 10 mg/L SMX in UPW, (b) HA matrix, (c) 10 mg/L SMX in HA matrix, (d) SW matrix, and (e)
512 10 mg/L SMX in SW matrix.

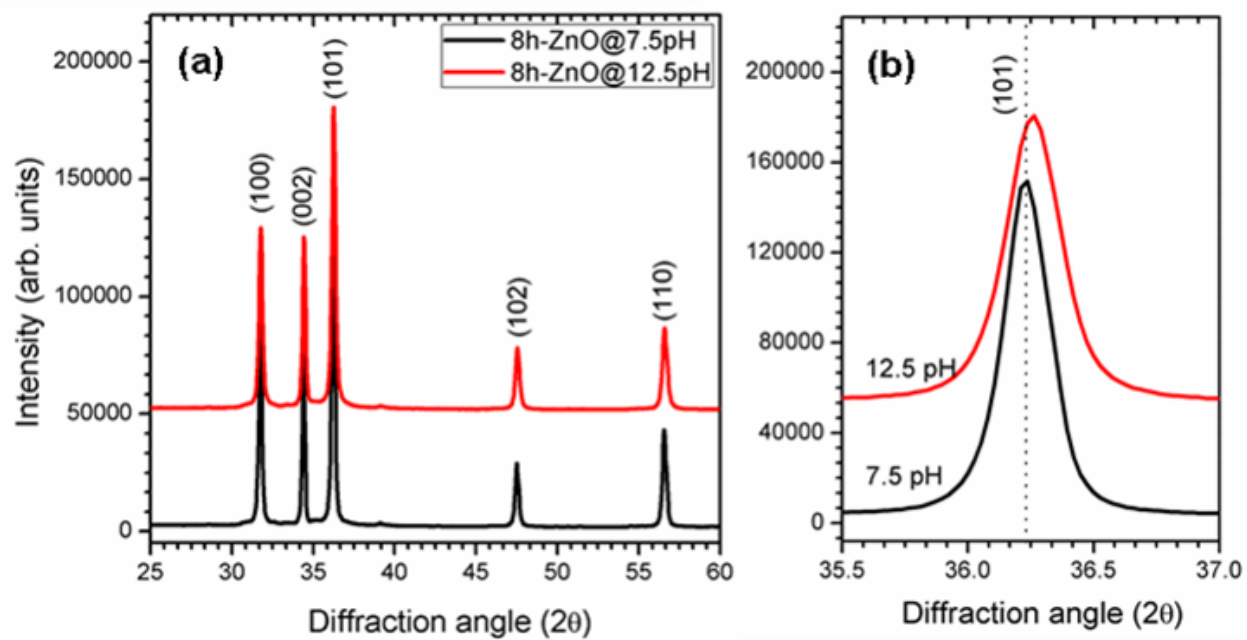
513 **Figure 9.** Evolution of the size of crystallite as a function of SMX initial concentrations and the
514 type of the water matrix.

515

516

517

518



519

520

521 **Figure 1.** (a) XRD patterns of ZnO nanostructures synthesized at pH 7.5 and 12.5, and (b) high
522 magnification showing a (101) plane with peak shift.

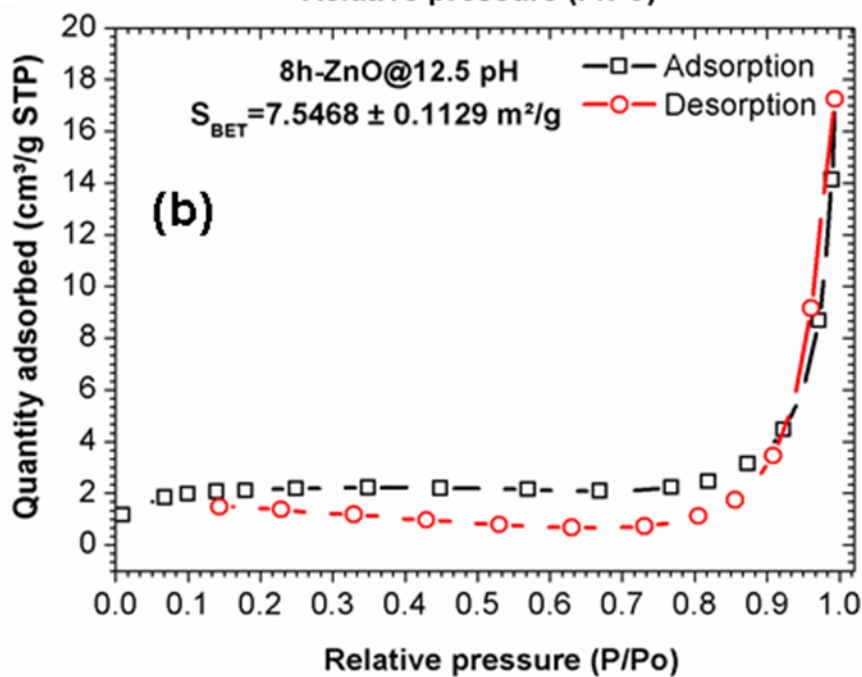
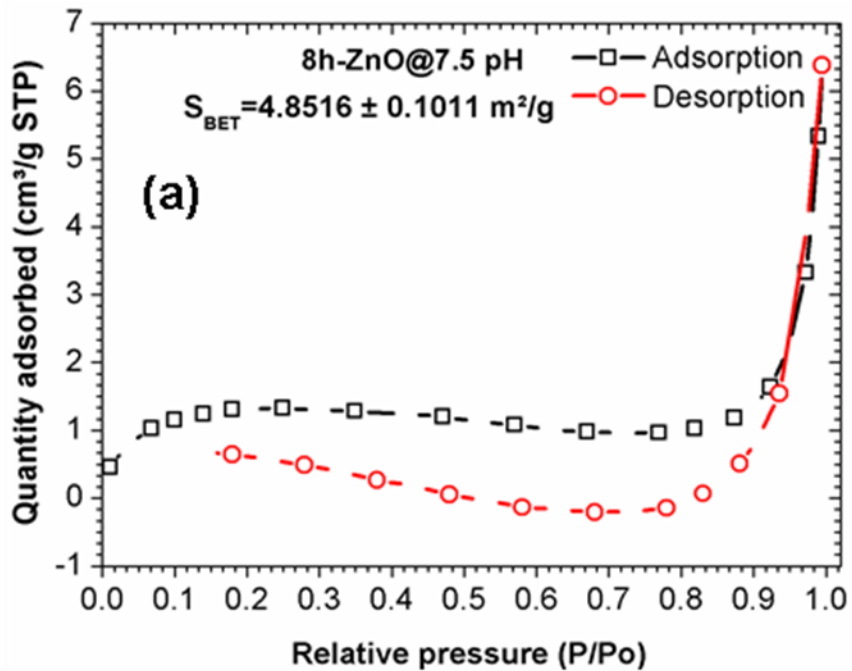
523

524

525

526

527

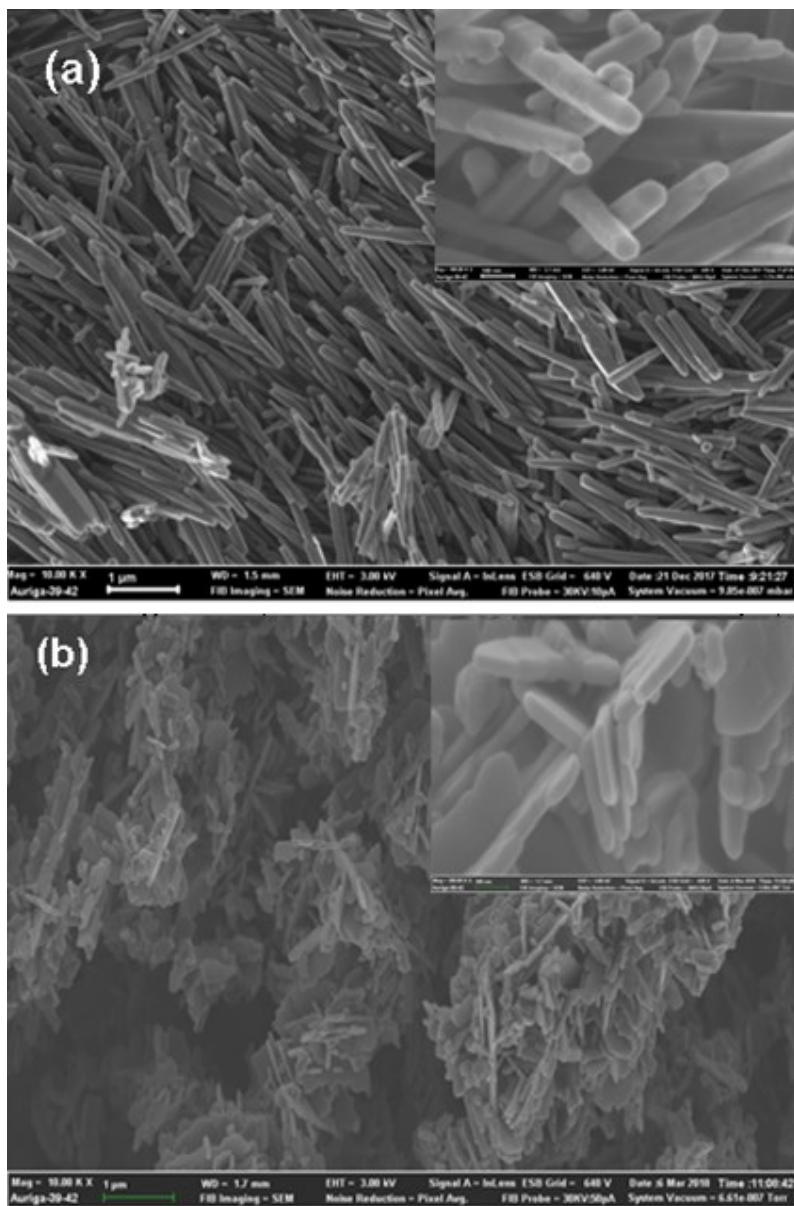


528

529 **Figure 2.** The N₂ adsorption/desorption isotherms of ZnO prepared at pH (a) 7.5 and (b) 12.5.

530

531



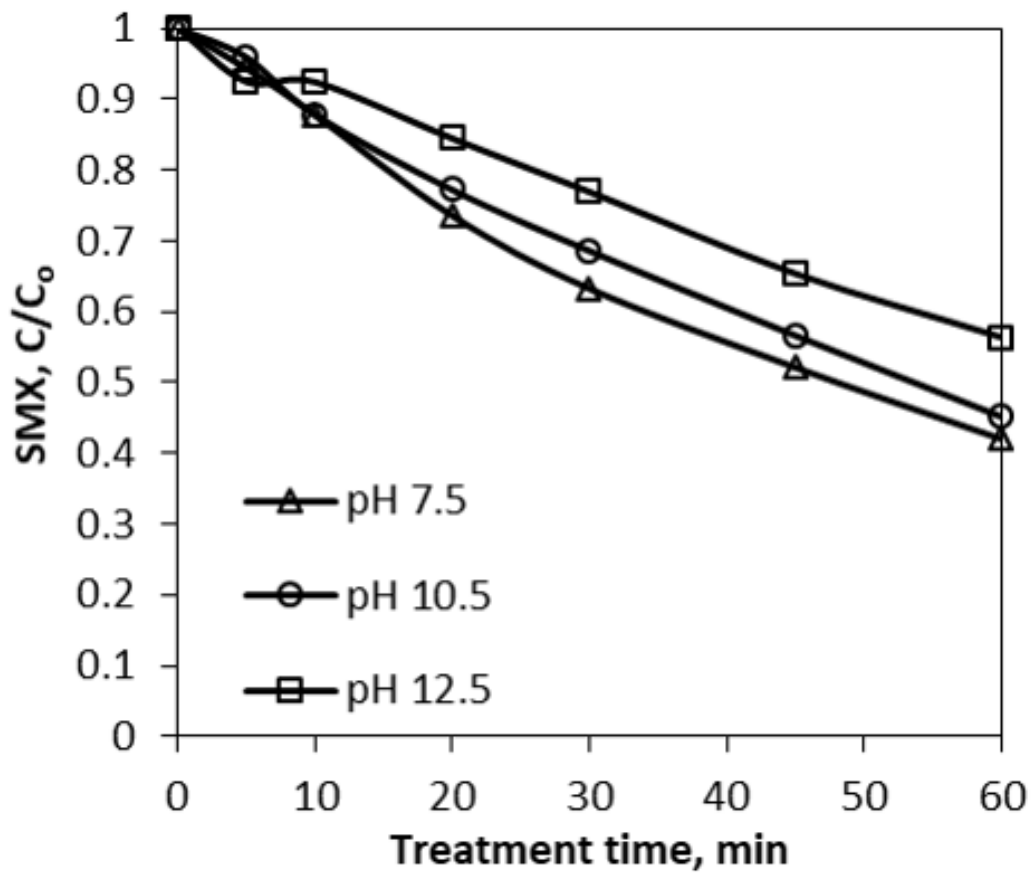
532

533 **Figure 3.** SEM micrographs of ZnO nanostructures prepared at (a) pH 7.5 and heated for 8 h,

534 and (b) pH 12.5 and heated for 8 h.

535

536



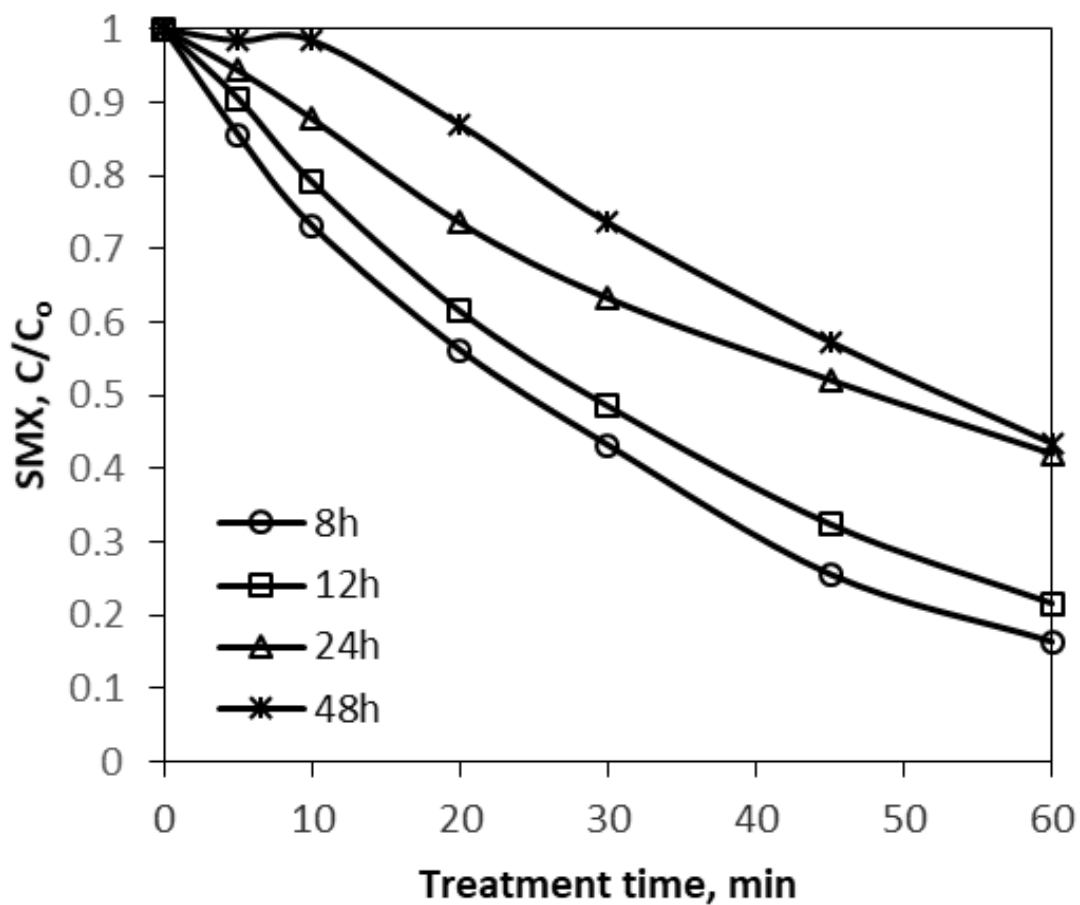
537

538 **Figure 4.** Effect of the pH of the ZnO synthesis reaction on the photocatalytic degradation of

539 SMX ($C_0=10$ mg/L, $C_{ZnO}=200$ mg/L, ZnO heating time: 24 h).

540

541



542

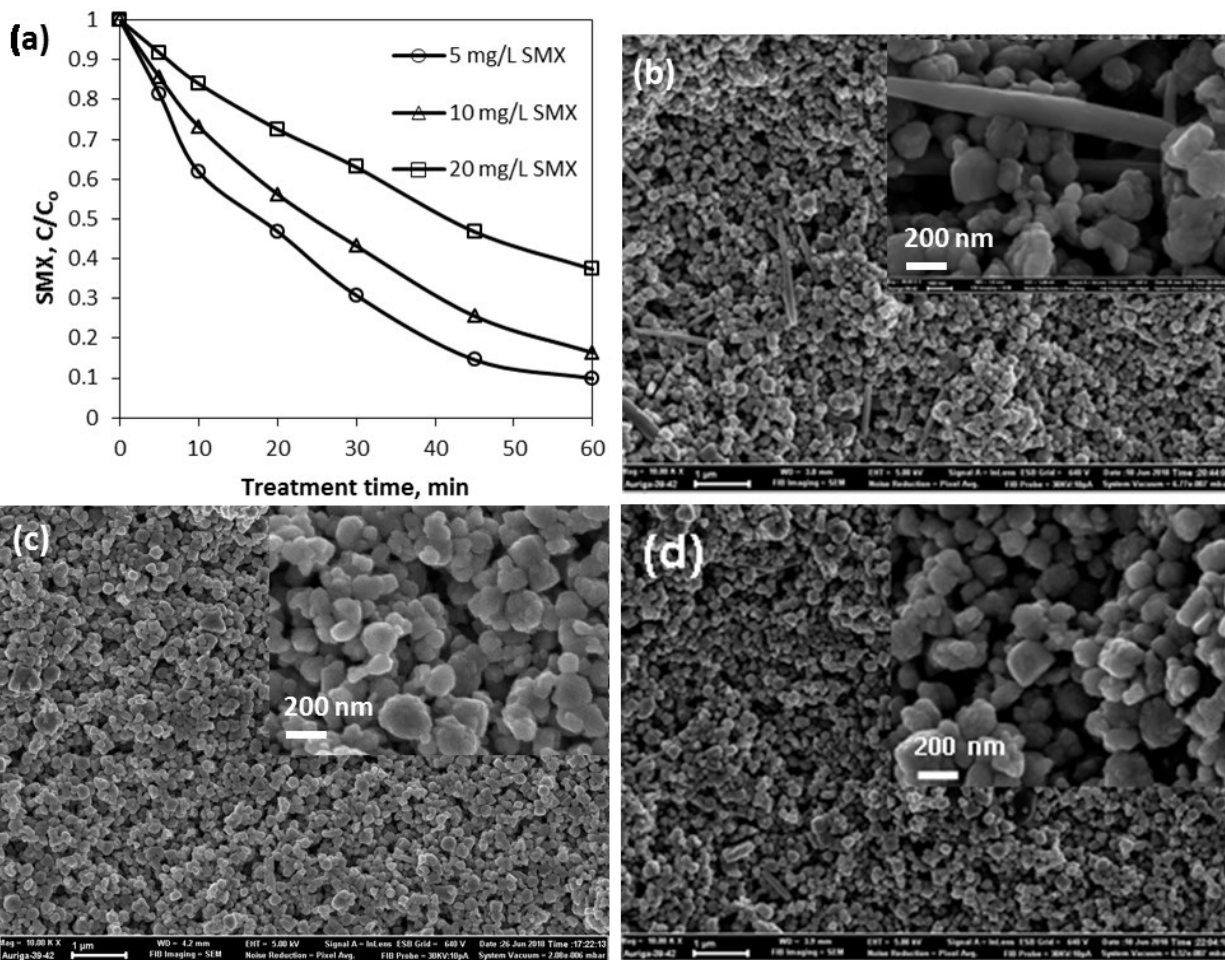
543 **Figure 5.** Effect of catalyst's heating time at 200 °C on the photocatalytic degradation of SMX

544 ($C_0 = 10$ mg/L, $C_{ZnO} = 200$ mg/L, catalysts' synthesis reaction pH = 7.5).

545

546

547



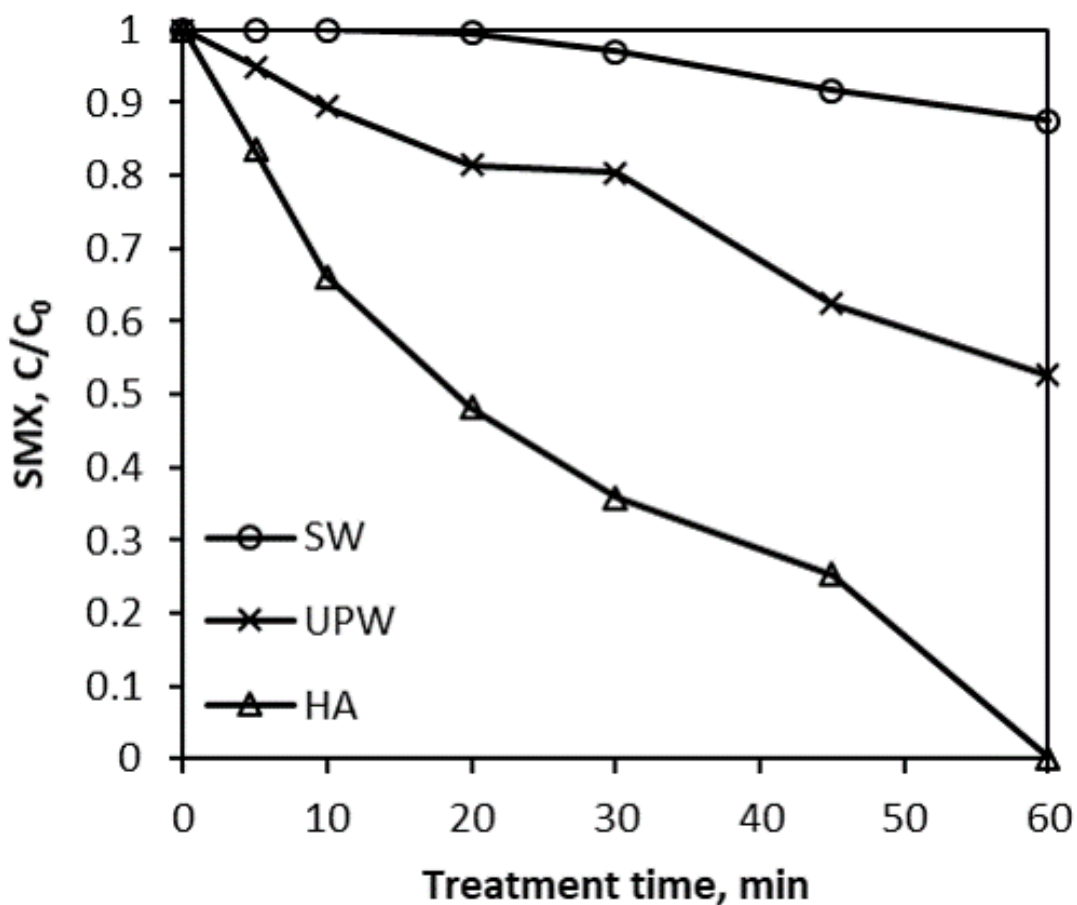
548

549 **Figure 6.** (a) Effect of initial SMX concentration on its photocatalytic degradation (ZnO-
 550 8h@7.5pH, $C_{ZnO} = 200$ mg/L), (b) SEM micrographs of ZnO-8h@7.5pH after 60 min of
 551 treatment at initial SMX concentration of 5 mg/L, (c) 10 mg/L, and (d) 20 mg/L.

552

553

554

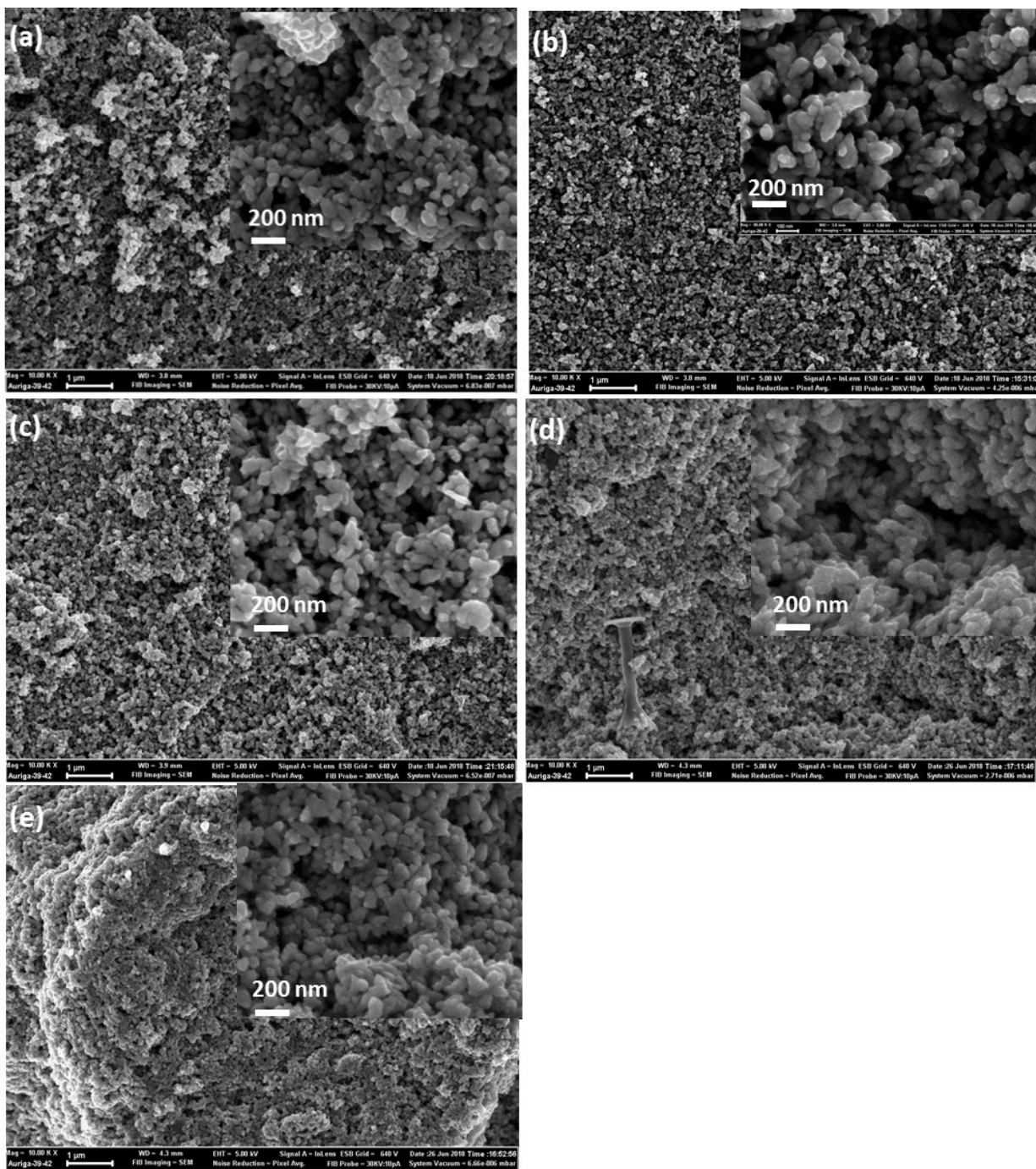


555

556 **Figure 7.** Effect of water matrix on the photocatalytic degradation of SMX ($C_0 = 10 \text{ mg/L}$, C_{ZnO}
 557 $= 200 \text{ mg/L}$, catalyst: ZnO-8h@12.5pH).

558

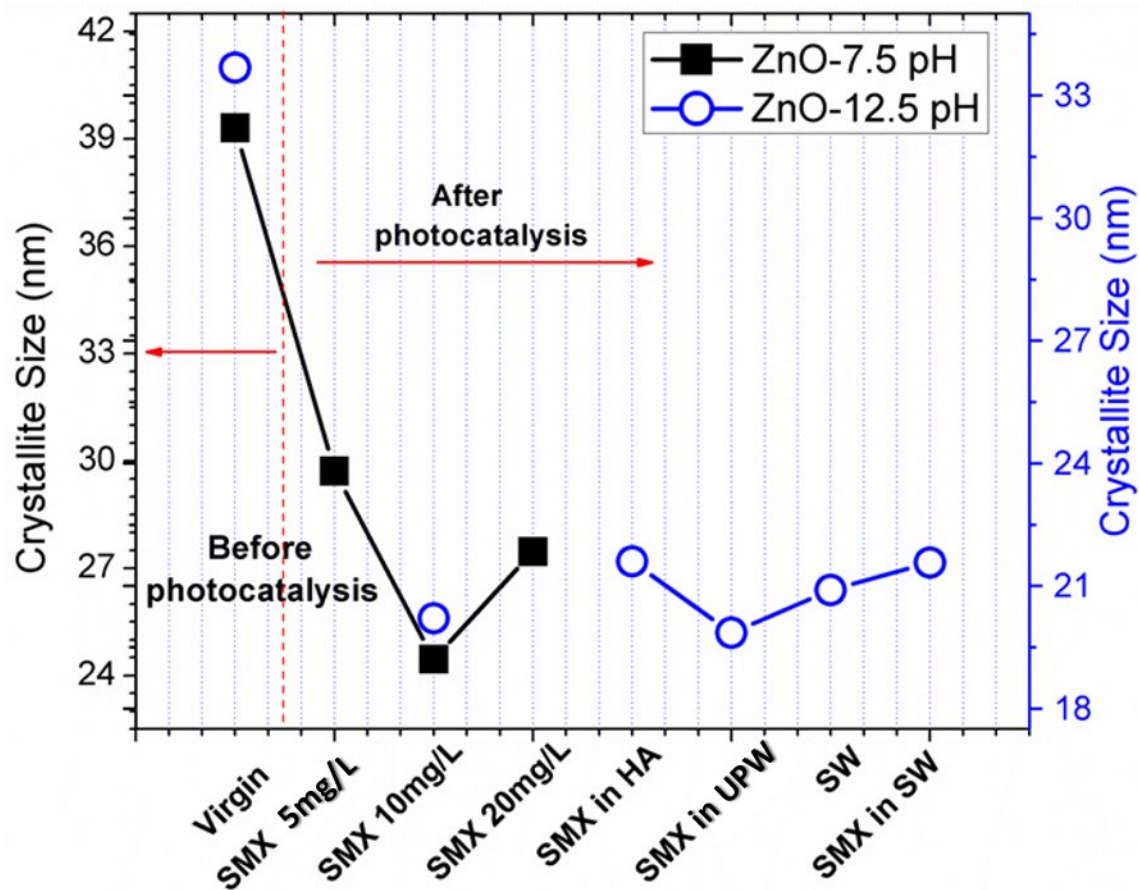
559



560

561 **Figure 8.** SEM micrographs of ZnO-8h@12.5pH after 60 min of treatment in the presence of (a)
 562 10 mg/L SMX in UPW, (b) HA matrix, (c) 10 mg/L SMX in HA matrix, (d) SW matrix, and (e)
 563 10 mg/L SMX in SW matrix.

564



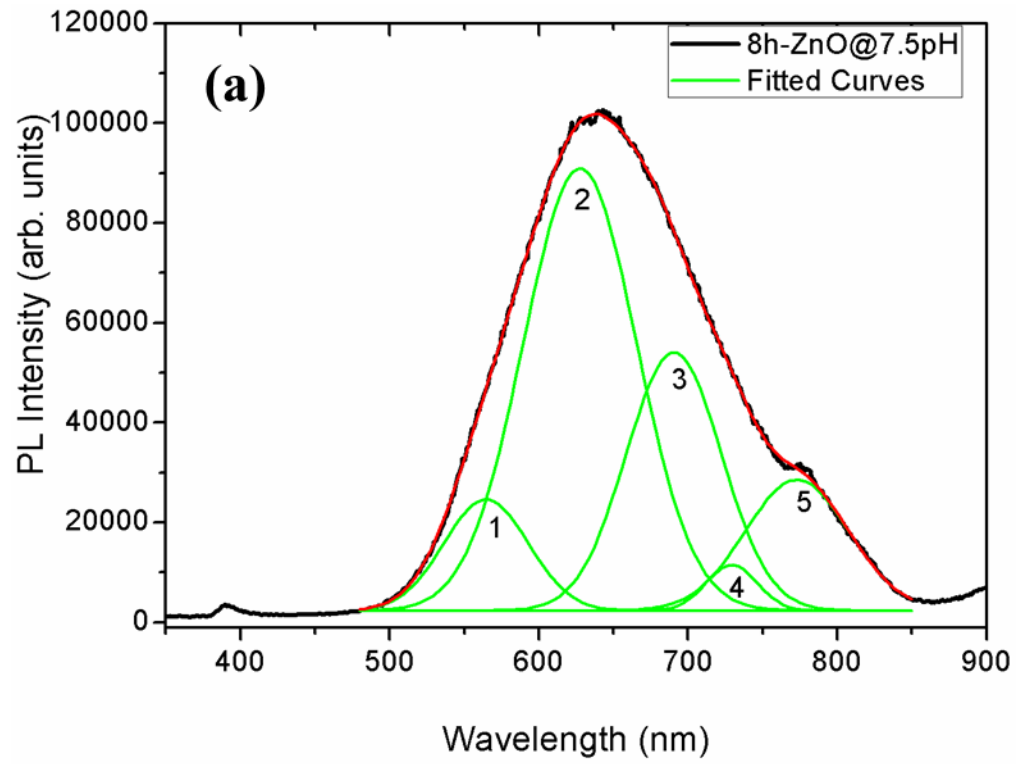
565

566 **Figure 9.** Evolution of the size of crystallites as a function of SMX initial concentrations and the
 567 type of the water matrix.

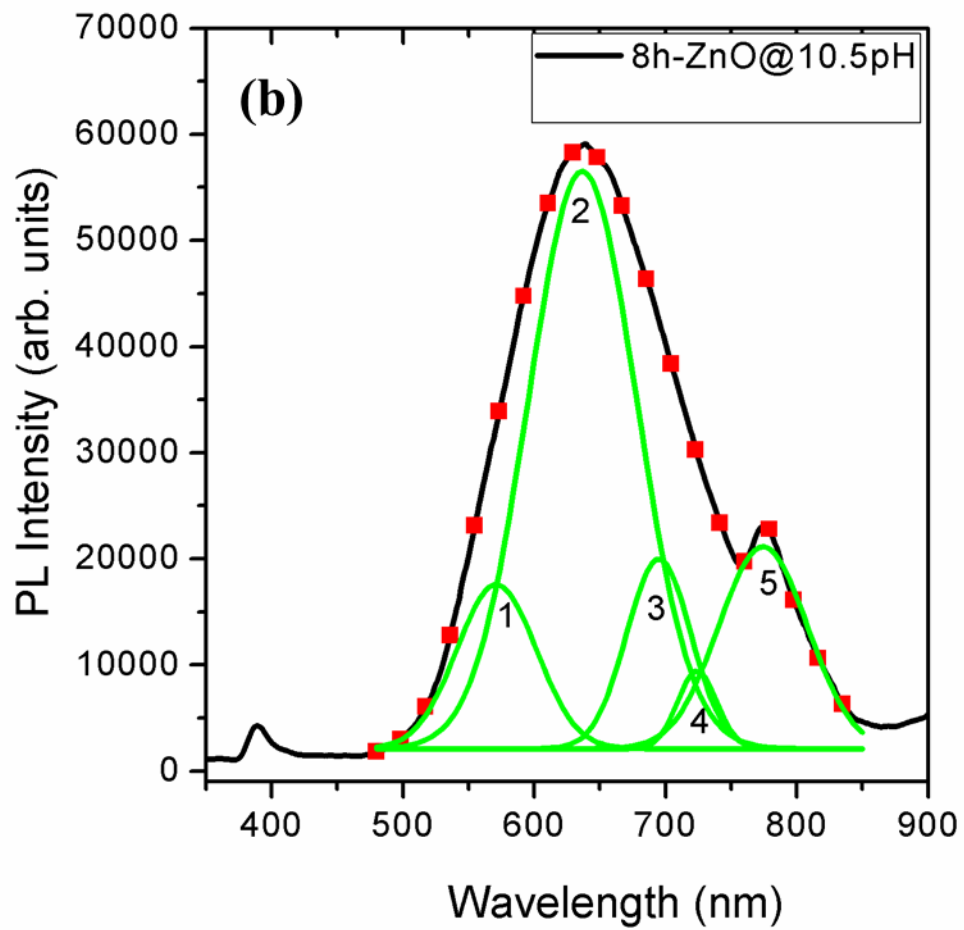
568

569

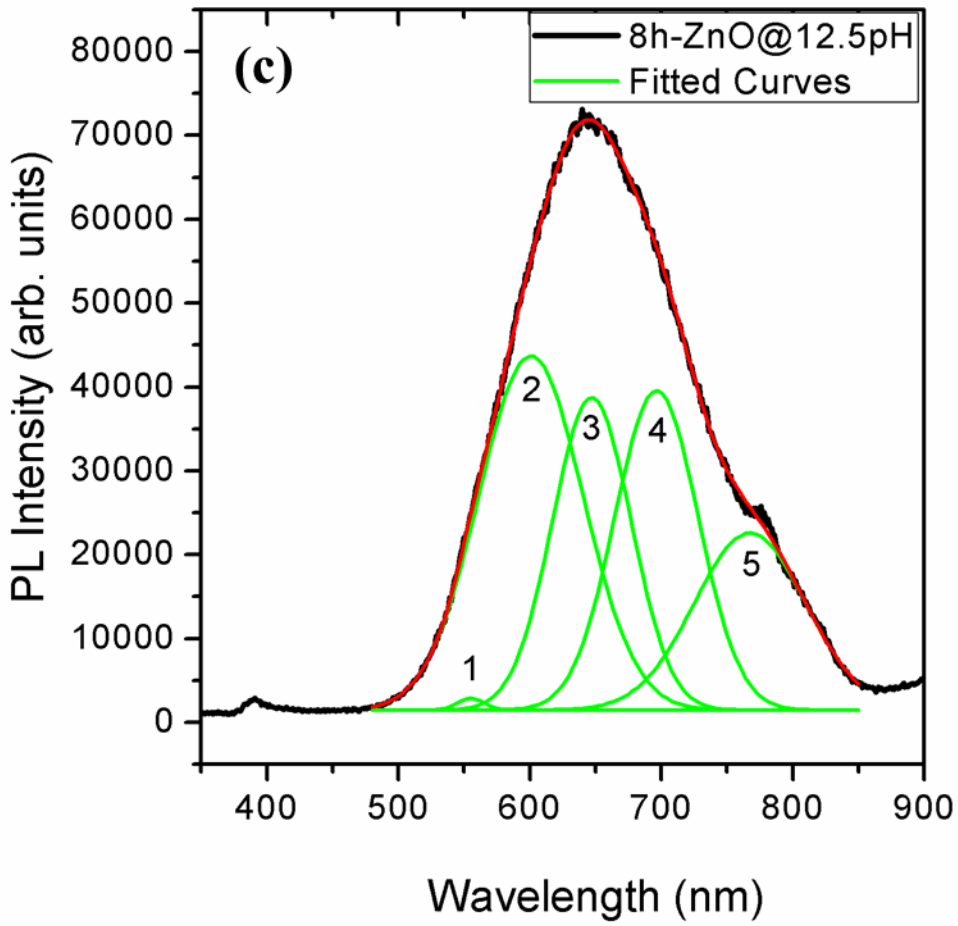
571



572



573



574

575 Figure S1. Photoluminescence (PL) spectra of the synthesized ZnO catalysts.

576